

New axion bounds derived from the 100-parsec Gaia DR3 white dwarf luminosity function

M. L. Alberino,^{a,b} M. M. Miller Bertolami,^{a,b} M. E. Camisassa,^c A. Caputo^{d,e,f} and S. Torres^c

^aInstituto de Astrofísica de La Plata, Consejo Nacional de Investigaciones Científicas y Técnicas Avenida Centenario (Paseo del Bosque) S/N, B1900FWA La Plata, Argentina

^bFacultad de Ciencias Astronómicas y Geofísicas, Universidad Nacional de La Plata Avenida Centenario (Paseo del Bosque) S/N, B1900FWA La Plata, Argentina

^cDepartament de Física, Universitat Politècnica de Catalunya, c/Esteve Terrades 5, 08860 Castelldefels, Spain

^dDepartment of Theoretical Physics, CERN, Esplanade des Particules 1, P.O. Box 1211, Geneva 23, Switzerland

^eDipartimento di Fisica, “Sapienza” Università di Roma & Sezione INFN Roma1, Piazzale Aldo Moro 5, 00185, Roma, Italy

^fDepartment of Particle Physics and Astrophysics, Weizmann Institute of Science, Rehovot 7610001, Israel

E-mail: mlalberino@fcaglp.unlp.edu.ar

Abstract. The axion, a well-motivated hypothetical particle arising in extensions of the Standard Model, can be produced copiously within the hot, compact cores of white dwarf stars. The shape of the white dwarf luminosity function (WDLF) is a powerful tool for constraining theoretical particles that would imply an additional cooling channel in white dwarfs. In this work, and for the first time, we use the 100-parsec *Gaia* DR3 white dwarf sample and compare it with theoretical predictions. We have simulated synthetic populations of white dwarfs using a population synthesis code based on Monte Carlo techniques, incorporating realistic observational errors, and based on state-of-the-art white dwarf models that incorporate the anomalous cooling caused by the presence of axions. Axion bremsstrahlung emission rates were implemented using the latest theoretical calculations. We find that, for the brightest white dwarfs in the sample ($M_{\text{bol}} < 10$), the χ^2 statistic is largely insensitive to the assumed stellar formation rate (SFR), which is typically the dominant uncertainty in modeling the Galactic-disk WDLF. The resulting χ^2 analysis disfavors a sizable additional cooling contribution. This conclusion contrasts with earlier studies in which axion–electron couplings in the range $0.7 \times 10^{-13} < g_{ae} < 2.1 \times 10^{-13}$ provided mildly improved fits to the Galactic-disk WDLF. We attribute the discrepancy to simplifying assumptions in previous modeling and to the substantially improved observational quality of the 100-pc *Gaia* DR3 sample. We obtain the upper limit $g_{ae} < 1.68 \times 10^{-13}$ (95% C.L.), which is among the strongest available.

Contents

1	Introduction	1
2	White dwarf models and input physics	3
2.1	Standard white dwarf physics	3
2.2	Axion emission in white dwarfs	3
2.3	Initial models and white dwarf model grid	4
3	Construction of the white dwarf luminosity function	6
3.1	Monte Carlo population synthesis code	6
3.2	Observed and theoretical white dwarf luminosity functions	7
3.3	The bright WDLF and its independence from the star formation history	9
4	Impact of the axion emission in the WDLF	10
5	Conclusions and future work	11
A	Effects of stellar formation bursts on the WDLF	13

1 Introduction

The axion was originally proposed as a compelling dynamical solution to the strong-CP problem in QCD [1–3], emerging as a pseudo-Nambu–Goldstone boson of a spontaneously broken global symmetry. Beyond this minimal motivation, a broad class of axion-like particles (ALPs) arises naturally in well-motivated extensions of the Standard Model, including many string-inspired constructions [4, 5], making light pseudoscalars a generic target for both particle-physics and astrophysical probes. Over roughly the past two decades, the axion field has experienced a major acceleration in both theoretical development and experimental activity. On the theory side, this includes increasingly systematic treatments of axion/ALP effective theories, production mechanisms, and their phenomenology across laboratory, astrophysical, and cosmological settings. On the experimental side, a diverse global program has formed, spanning haloscope searches for Galactic dark-matter axions, helioscopes targeting solar axions, purely laboratory “light-shining-through-walls” techniques, and a growing portfolio of novel detection concepts exploiting electromagnetic, nuclear, and condensed-matter technologies. Comprehensive overviews of this rapidly evolving landscape can be found in recent reviews [6–11]. A powerful and largely complementary avenue comes from stellar evolution. If axions couple to Standard Model particles, they can be produced efficiently in stellar interiors and escape, providing an additional energy-loss channel that alters cooling times and, consequently, various stellar observables [11–13]. White dwarfs are particularly attractive laboratories in this context: their late-time evolution is essentially a cooling process, and the white dwarf luminosity function (WDLF) is especially sensitive to the cooling rate. This connection has motivated a long line of studies using white dwarfs—via both WDLF measurements [14–16] and white dwarf pulsation properties [17–20]—to test axion-induced cooling. In particular, the WDLF provides a powerful probe of light pseudoscalars with an electron coupling. In white dwarfs, these particles would be emitted predominantly

through a Bremsstrahlung process, and would act as a non-negligible extra-cooling for the brightest and youngest white dwarfs [14–16].

In the specific case of the QCD axion, the axion–electron coupling arises in concrete ultraviolet completions such as the DFSZ model [21, 22]. In DFSZ realizations one may express the coupling as

$$g_{ae} = 2.8 \times 10^{-14} \left(\frac{m_a}{\text{meV}} \right) \cos^2 \beta, \quad (1.1)$$

where m_a is the axion mass and $\cos^2 \beta$ is a model-dependent parameter. For generic ALPs, instead, g_{ae} and the ALP mass are independent parameters, and for a given axion mass the WDLF constrains g_{ae} directly.

Using WDLF determinations based on white-dwarf samples from the Sloan Digital Sky Survey (SDSS) and the SuperCOSMOS Sky Survey (SSS), [15] reported an upper bound $g_{ae} < 2.3 \times 10^{-13}$ at 95% confidence level. Moreover, analyses of these earlier WDLFs [15, 16] found a modest improvement in the fit for axion masses in the range $2.5 < m_a \cos^2 \beta < 7.5$ meV. It is also worth noting that the WDLF employed in these analyses are based on magnitude-limited samples, using the $1/V_{max}$ method [23] to account for the incompleteness of the sample at low luminosities [24, 25]. In this method, each star is counted weighted by $1/V_{max}$, where V_{max} is the maximum volume where the star would still be visible considering the magnitude cut of the sample. This way, fainter stars contribute more to the WDLF than brighter stars. Although this method has been widely used in past decades, recent advances in the observed population of white dwarfs have allowed the construction of volume-limited samples. Indeed, the *Gaia* space mission has provided a 100 pc volume-limited sample that reaches $\sim 94\%$ for a parallax relative error lower than $\sim 10\%$ [26]. Once a proper classification of the distinct Galactic populations [27] and spectral classifications are performed [28–30] this sample allows the construction of a WDLF exempt from typical observational biases present in magnitude-limited samples [see e.g. 28, 31]. Furthermore, these previous analyses of axion properties using WDLFs adopted proper-motion selection methods, while *Gaia* parallax measurements have enabled the determination of distances and absolute magnitudes for these stars. Also, new classification techniques based on Random Forest algorithms that use the full parameter space of the observations are now available to separate those white dwarfs that belong to the Galactic thin disk [27].

Owing to unaccounted observational biases and modeling assumptions in the construction of old theoretical WDLFs, previous constraints on axion properties are likely overestimated. Moreover, recent revisions of axion emissivities [32] indicate that the emission rates previously reported in the literature [33, 34] were also slightly overestimated. The high quality of the 100 pc volume limited white dwarf sample of the *Gaia* DR3 sample [28] opens the possibility of improving the quality and robustness of previous constraints. Achieving this goal, however, requires a faithful propagation of observational uncertainties in the comparison between data and theory. The best way to achieve this is by means of Monte Carlo population-synthesis simulations, in which one generates synthetic white dwarf populations and constructs the corresponding WDLF while folding in the *Gaia* performance characteristics (astrometric and photometric uncertainties, completeness, and selection function) in a forward-modeling framework. Moreover a proper set of cooling white dwarf models in which axion emission is computed self-consistently with the thermal structure of the stars, following the approach advocated by [15], is desirable. In the present work we implement this strategy and apply it to the *Gaia* DR3 100 pc sample.

The paper is organized as follows: In Section 2, we discuss the axion emission rates and the computation of stellar models. In Section 3 the generation of synthetic populations. In Section 4, we quantitatively assess the impact of axions on the theoretical WDLF and provide statistical tests to constrain g_{ae} at the 95% confidence level. Finally, in Section 5, we summarize our results and conclusions and outline possible directions for future work.

2 White dwarf models and input physics

2.1 Standard white dwarf physics

The stellar evolution computations presented on this work were carried out with the LPCODE stellar evolution code, widely used in the study of different problems related to the evolution of white dwarfs [35–37]. A detailed description of the code is available at [36] and references therein. The equation of state for the high- and low-density regimes are taken from [38] and [39], respectively. Conductive opacities are those of [40] while radiative opacities are those of the OPAL project [41] complemented at low temperatures by the molecular opacities produced by [42]. White dwarf models computed with LPCODE also include detailed non-gray model atmospheres to provide accurate boundary conditions for our models, which include non ideal effects in the gas equation of state, see [43] for details. Neutrino cooling by Bremsstrahlung, photo and pair production are included following the recipes of [44], while plasma processes are included according to [45]. All relevant energy sources are taken into account in the simulations, including residual nuclear burning, the release of latent heat and the gravitational energy associated with the phase separation in the carbon-oxygen profile induced by crystallization. The inclusion of all these energy sources is done self-consistently and locally coupled to the full set of equations of stellar evolution. In addition, time-dependent element diffusion during white dwarf evolution is taken into account following the treatment of multicomponent gases of [46] and the fully implicit numerical approach presented in [47], including thermal, chemical, and gravitational diffusion; and taking into account the effects of Coulomb interactions on the gravitational settling [48]. For the present work we considered the diffusion of H, ^2H , ^3He , ^4He , ^{12}C , ^{13}C , ^{14}N , ^{16}O , and ^{22}Ne .

2.2 Axion emission in white dwarfs

If axions are coupled to electrons, the dominant emission process in white dwarfs is electron-ion Bremsstrahlung [49–51]. This process take place in a highly degenerate environment and is also characterized by strong ion-correlations ($\Gamma \gg 1$)¹. The treatment of Bremsstrahlung emission for such a regime has been accounted as in [32], who have recently reviewed the bremsstrahlung emission of bosons in degenerate environments, including axions. Specifically, Bremsstrahlung axion emission was computed as

$$\epsilon_{BD} = 10.85 \alpha_{26} T_8^4 \sum_j^{N_{\text{isot}}} \frac{X_j Z_j^2}{A_j} \times F_j, \quad (2.1)$$

¹The ionic coupling constant (Γ) for multicomponent plasmas is defined as

$$\Gamma = 2.275 \times 10^5 \frac{(\rho Y_e)^{1/3}}{T} \sum_i (n_i/n_{\text{ions}}) Z_i^{5/3} \quad [\text{c.g.s.}],$$

where the sum is taken over all considered nuclear species.

	a_0	a_1	a_2	a_3
	b_0	b_1	b_2	b_3
Helium				
($Z = 2$)	+0.413	+0.233	-0.655	+0.058
	+0.931	+0.096	-2.641	+1.226
Carbon				
($Z = 6$)	+0.248	+0.306	-1.145	+0.393
	+1.293	+0.152	-2.918	+1.200
Oxygen				
($Z = 8$)	+0.133	+0.325	-1.155	+0.410
	+1.401	+0.169	-3.006	+1.213
Neon				
($Z = 10$)	+0.016	+0.335	-1.081	+0.384
	+1.495	+0.184	-3.121	+1.248

Table 1. Coefficients for the fit functions of eqs. (2.3).

where α_{26} is the axionic fine structure constant², $T_8 = T/10^8$ and X_j , Z_j and A_j are the mass fraction, atomic number and atomic weight of element j . The function F_j is being computed as

$$F_j(x, \Gamma) = \mathcal{A}_j(x)\Gamma^{-0.37} + \mathcal{B}_j(x)\Gamma^{+0.03} \quad (2.2)$$

in the case $1 < \Gamma < 160$ and $4 < \log_{10} \rho < 7$, where ρ is the density in units of g/cm^3 , $x = \log_{10}(\rho)$, and

$$\begin{aligned} \mathcal{A}_j(x) &= a_o^j + a_1^j x + \frac{a_2^j}{(8-x)} + \frac{a_3^j}{(8-x)^2} \\ \mathcal{B}_j(x) &= b_o^j + b_1^j x + \frac{b_2^j}{(8-x)} + \frac{b_3^j}{(8-x)^2} \end{aligned} \quad (2.3)$$

are fit functions. These fitting functions are accurate at the few-percent level over their range of applicability and improve on recipes used in earlier studies. Table 1 shows the values of the coefficients computed by [32] for carbon and oxygen, together with the values for neon and helium that were computed specifically for the present work. On strong ion-correlation environments where the conditions established on [32] were not met we used the prescriptions derived in [33, 34].

The full set of axion recipes used in our code includes axion emission by Compton process, bremsstrahlung emission in the non-degenerate case as in [13], and at low ion-correlations in the degenerate case we used [52]. For intermediate ion-correlations ($0.9 < \Gamma < 1.1$) we interpolated linearly between recipes, and for intermediate degeneracy, which is of more relevance in stars from the Red Giant Branch (RGB) and the Asymptotic Giant Branch (AGB) than in white dwarfs [53], we interpolate with a harmonic expression as in [15].

2.3 Initial models and white dwarf model grid

The initial white dwarf models adopted in our simulations were taken from [54]. These models represent the initial states of the white dwarfs whose surfaces will be dominated by

² g_{ae} is also related to the axionic fine structure constant α_{26} by $\alpha_{26} = 10^{26} g_{ae}^2 / 4\pi$.

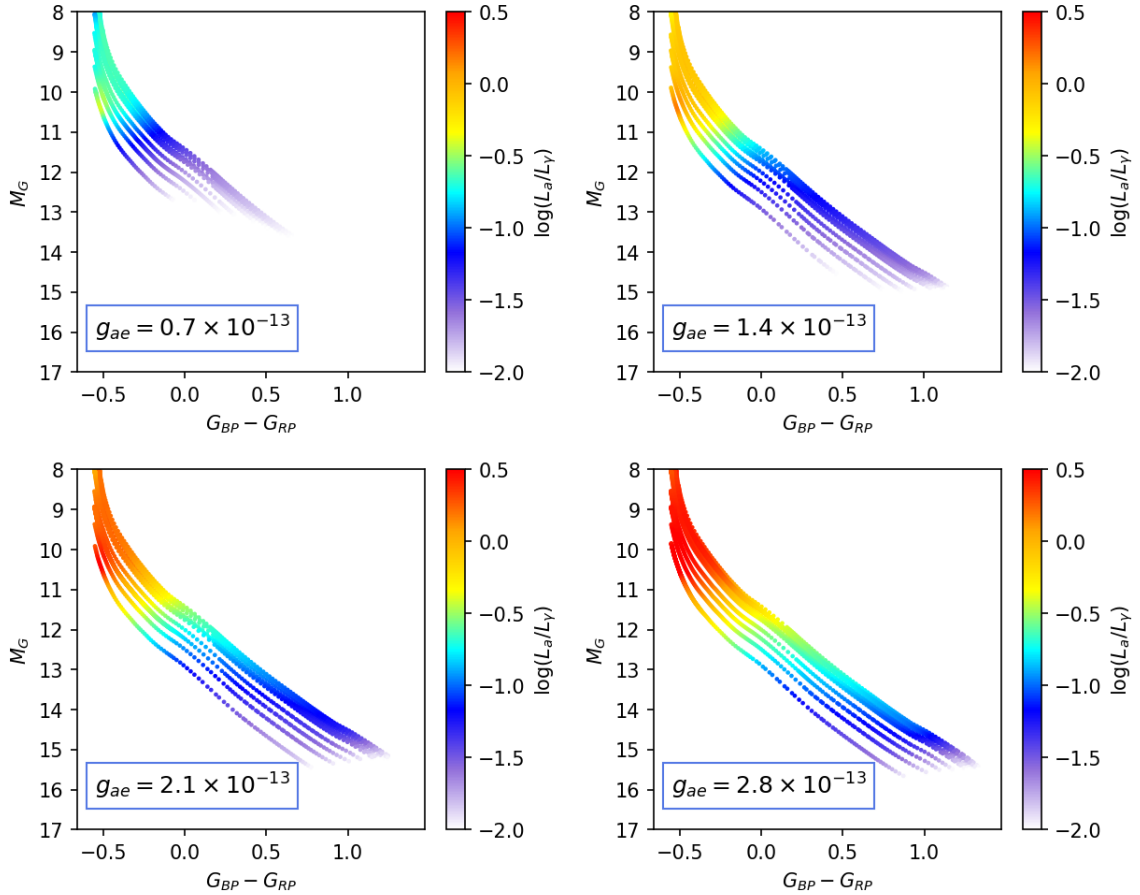


Figure 1. Evolutionary tracks of white dwarfs with $Z = 0.01$ and masses in the range $0.48\text{--}1.05 M_{\odot}$. Each panel considers different values of g_{ae} . The color scale shows the intensity of axion emission relative to the surface luminosity.

hydrogen, i.e. DA white dwarfs. The initial metallicities considered in these models were $Z = 0.0001$, $Z = 0.001$, $Z = 0.01$, and $Z = 0.02$. Interpolation between these values is sufficient to generate theoretical models for white dwarfs with metallicities typical of stellar clusters, the solar neighborhood, and even the Galactic halo. The pre-white dwarf models were calculated in [54] for a set of given masses for the main-sequence progenitors, and are the result of the computation of the full previous evolution under the assumption of grounded wind prescriptions. Consequently, evolutionary computations do not yield neatly rounded white dwarf masses; rather, their values contain many decimals and differ for each metallicity. To improve the efficiency of interpolations between different evolutionary tracks in the Monte Carlo simulations, we rescaled the white dwarf masses—i.e., we changed the total mass of the white dwarfs keeping the chemical gradient fix in term of $m(r)/M_{\text{tot}}$ —constructing a grid of initial models with white dwarf masses of $0.48, 0.50, 0.53, 0.56, 0.58, 0.60, 0.70, 0.80, 0.90$ and $1.05 M_{\odot}$ for each metallicity. This procedure is justified because the net change in stellar mass before and after the rescaling is small, and the differences to the chemical stratification are negligible when compared with the current uncertainties in prior stellar evolution (e.g., the initial-to-final mass relation, which is sensitive to poorly constrained processes such as mass loss and convective overshooting). Then we calculated the white dwarf evolutionary

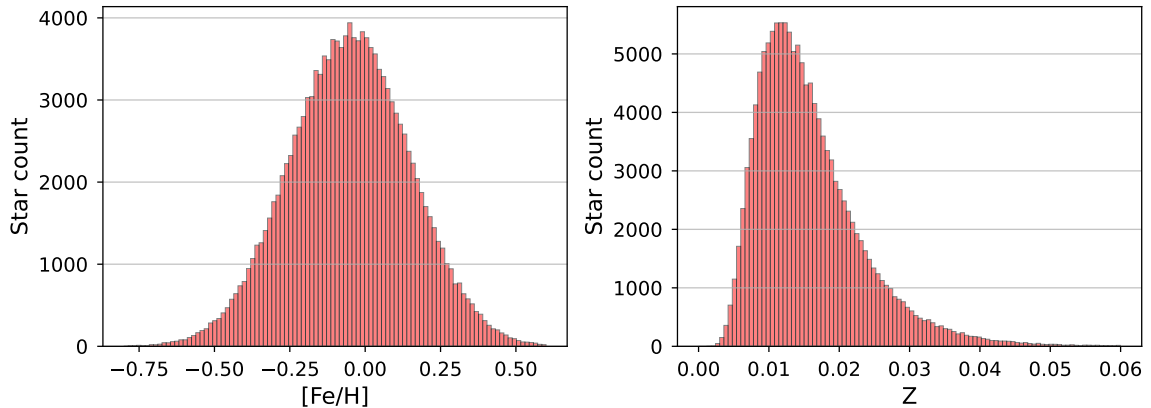


Figure 2. Left panel: Metallicity Distribution Function (MDF) of the solar neighborhood in terms of $[\text{Fe}/\text{H}]$, in agreement with [55]. Right panel: Z distribution, related to $[\text{Fe}/\text{H}]$ via $Z = Z_0 \cdot 10^{[\text{Fe}/\text{H}]}$, where we used $Z_0 = 0.016$ as the total solar metallicity, according to [56].

models, considering several values of the coupling constant g_{ae} between 0 and 8.4×10^{-13} , that translates, in terms of $m_a \cos^2 \beta$ under Eq. 1.1, to: 0, 2.5, 5, 7.5, 10, 12.5, 15, 20 and 30 meV. Therefore calculating 360 white dwarf models. Fig. 1 shows the evolutionary tracks for $Z = 0.01$ corresponding to the grid masses and for different values of the axion-electron coupling constant g_{ae} .

3 Construction of the white dwarf luminosity function

3.1 Monte Carlo population synthesis code

To construct the theoretical WDLFs for the Galactic disk we made use of the Monte Carlo population synthesis code [57] for synthetic white dwarf populations. This code has been widely used in the analysis of single [e.g. 26, 58–60] and binary [e.g. 61–64] populations of white dwarfs, as in studies of open and globular clusters [e.g. 65, 66] and the Galactic bulge [67]. A detailed description of the code can be found in these references. Therefore, we will only review its basic inputs.

Synthetic main sequence stars are generated with masses randomly following an initial mass function with a Salpeter distribution³ and a minimum mass of $0.4M_\odot$. Moreover, main sequence stars are generated at different initial times according to a given Stellar Formation Rate (SFR). Once every main-sequence star is generated, the BaSTI pre-white dwarf database [69] is employed to determine which stars had the time to become WD. Then, an initial-to-final-mass relation (IFMR) is adopted to compute the resulting white dwarf masses and cooling times. In the present work, we used the IFMR presented in [70]. To account for the Galactic disk metallicity, we used a bell-shaped curve for the Metallicity Distribution Function (MDF) of the solar neighborhood in terms of $[\text{Fe}/\text{H}]$, in agreement with the one presented in Fig. 15 of [55] and Fig. 5 of [71], related to Z via $Z = Z_0 \cdot 10^{[\text{Fe}/\text{H}]}$, where we used $Z_0 = 0.016$ as the total solar metallicity, according to [56]. The resulting MDF and the corresponding distribution in Z are shown in Fig. 2.

³The Salpeter initial mass function gives the number of stars $N(m)$ formed with masses in the range $(m, m + dm)$ as a power law of the form $N(m)dm \propto m^{-2.35} dm$ [68]

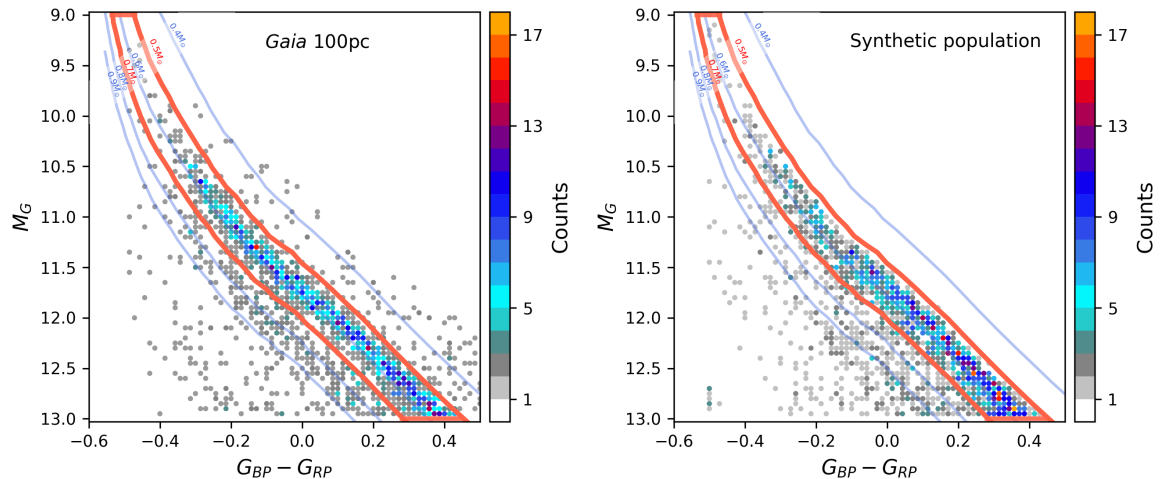


Figure 3. Hess diagrams for the *Gaia* 100-pc DA white dwarf sample from [28] (left panel), against a synthetic thin-disk DA white dwarf population of equal number of objects. Thin blue lines indicate the evolutionary tracks of white dwarfs of different masses. From top to bottom, 0.4, 0.5, 0.6, 0.8 and $0.9 M_{\odot}$. The red lines define the selected region of the color-magnitude diagram.

We considered that all white dwarfs have a thick H envelope, belonging to the DA spectral type. To determine the current status of a white dwarf of given mass and cooling times, we interpolate between the precomputed white dwarf model grids to obtain luminosity, effective temperature, surface gravity, and radius of the WD.

Finally, in order to compare with the observational sample, the Monte Carlo code applies atmospheric models [72] to convert the quantities of our stellar models into *Gaia passbands* magnitudes, and incorporates photometric and astrometric errors in concordance with *Gaia* performance⁴. Figure 3 shows a comparison between the observed color-magnitude diagram and a theoretical counterpart constructed with the same number of objects as the *Gaia* sample. Absolute magnitudes M_G correspond to the standard *Gaia* broad G band, while the color index $G_{BP} - G_{RP}$ is computed from *Gaia*'s blue (G_{BP}) and red (G_{RP}) photometric passbands. Along the white-dwarf cooling sequence, decreasing M_G values correspond to higher luminosity, while the color $G_{BP} - G_{RP}$ provides a proxy for the effective temperature (smaller values, indicate hotter objects). The colored density map (Hess diagram) encodes the number of objects per bin in this plane, and the thin blue curves indicate representative theoretical cooling tracks for different white-dwarf masses.

3.2 Observed and theoretical white dwarf luminosity functions

The observational sample that we will use to compare our theoretical simulations is the 100 pc *Gaia* DR3 white dwarfs sample from [28], that belong to the Galactic disk according to [27]. DA white dwarfs are better classified in the hotter regions of the color-magnitude diagram, where the spectral lines are more easily discernible (see [28]). Moreover, the axion emission is relevant on the brighter portion of the WDLF, as we can see in Fig. 1. Using the classification of [28], we analyzed the probability of a given star of belonging to the DA group. This probability is displayed in the color-magnitude diagram in the left panel of

⁴<http://www.cosmos.esa.int/web/gaia/science-performance>

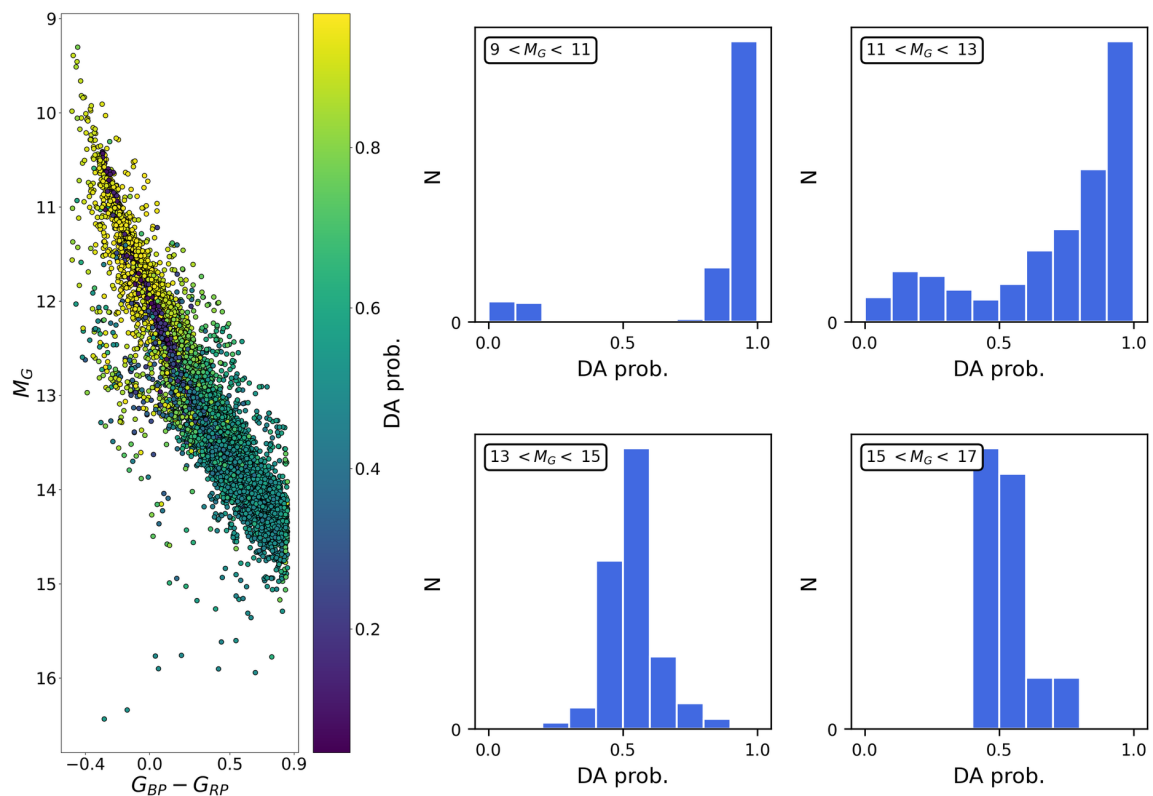


Figure 4. left panel: the color-magnitude diagram of the 100 pc white dwarf population classified into DA and non-DA by [28]. Color palette indicates the DA probability of each WD. Right panels: DA prob. distribution histograms for $9 < M_G < 11$, $11 < M_G < 13$, $13 < M_G < 15$, and $M_G > 15$.

Fig. 4. In the right panels of Fig. 4 we can see that the data exhibit a clear bimodality up until magnitudes $M_G < 13$, in which the two modes can be separated by a line at 0.5 in the DA probability, allowing us to statistically separate DA and non-DA white dwarfs. Beyond this magnitude, the spectral classification method is not good enough to tell DAs from non-DAs, as the probability distribution becomes unimodal. Alternatively, [29] constructs a DA sample based on [28] using a Random Forest algorithm. We present our final results following each of these approaches in the construction of the observational sample.

The next step in this process is to generate a theoretical WDLF for the Galactic disk under the assumption of different intensities for the coupling constant g_{ae} . The synthetic population of white dwarfs is sensitive to the specific form of the SFR, which must be prescribed within the Monte Carlo code. In the next section, we briefly review our knowledge of the Galactic disk SFR, discuss its prescription, and outline the associated problems.

Given that we are restricting the modelling to CO-core DA white dwarfs coming from single stellar evolution, we need to minimize as much as possible the contribution from binary stellar evolution channels (post-merger and post-Roche lobe overflow white dwarfs), as well as those white dwarfs formed by Super AGB stars, in the observational sample. This can be achieved by excluding from the sample He-core white dwarfs, as well as massive CO-core and ONe-core white dwarfs. In light of this, when constructing the WDLF we have then restricted our observational sample to those white dwarfs in the region delimited by the 0.5 and the 0.7

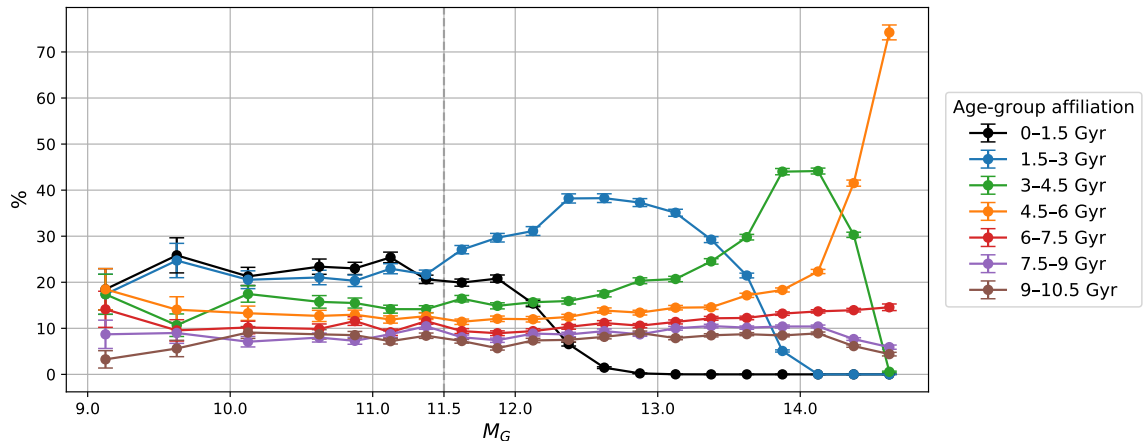


Figure 5. Contribution of different stellar age bins (0–1.5 Gyr, 1.5–3 Gyr, 3–4.5 Gyr, 4.5–6 Gyr, 6–7.5 Gyr, 7.5–9 Gyr and 9–10.5 Gyr) to each magnitude bin in the WDLF.

M_\odot white dwarf evolutionary tracks, brighter than $13 M_G$, and having $P(DA) > 0.5$. The region of the color-magnitude diagram finally considered for the construction of the WDLF is delimited by the red lines in Fig. 3.

3.3 The bright WDLF and its independence from the star formation history

The SFR of the Galactic disk in the solar neighborhood is poorly constrained (see, for example, Fig. 9 of [73]). This is not only due to our understanding of the Galactic stellar formation history, but also due to the complications that arise from stellar migration [74]. Previous works lead to discrepant results regarding the intensity and timing of stellar formation bursts within the Galactic disk, although they agree that the SFR has not varied by more than a factor 6 with bursts showing typical timescales of Gyrs. Within this context, it is a reasonable assumption to adopt a constant SFR for the whole history of the Galactic disk, i.e. the SFR is adopted as a step function, where the step location is defined by the assumed age of the Galactic disk, and normalization is a free parameter. This SFR is not short of problems when compared to the observed WDLF, given that the later exhibits some evidence of bursts in the recent formation rate history [75, 76], however, it involves a minimal set of assumptions and is therefore particularly suitable for the present work. Here we have adopted a constant SFR for a Galactic disk of 10.6 Gyr of age, consistent with [77]. Moreover, in the absence of very recent, short-lived bursts of star formation (shorter than 0.5 Gyr; see [78]), for which there is no observational evidence [73], the brightest portion of the WDLF ($M_G \lesssim 11.5$) is expected to be largely independent of the SFR [79, 80], making this region particularly well suited for robust statistical tests on additional cooling channels, since the SFR constitutes our main source of uncertainty. In contrast, extending the analysis to fainter magnitudes, $M_G \gtrsim 11.5$, would be unsuitable for such statistical tests, given the current level of uncertainty in the SFR, as discussed in Appendix A.

In order to test the independence of the theoretical WDLF—constructed here via Monte Carlo simulations—from the SFR at the bright end, we computed the fractional contribution of progenitors formed in seven stellar age bins—each spanning 1.5 Gyr—to each magnitude bin of the WDLF. Figure 5 shows the resulting distributions. We find that up to $M_G \simeq 11.5$ the relative contributions of the different age bins remain nearly invariant within Poisson

uncertainties, indicating that the bright WDLF is insensitive to the SFR. Only at fainter magnitudes do progressively older stellar populations begin to dominate, and the age distributions cease to be invariant. This numerical experiment therefore confirms that, in the bright region considered here and in the restricted white dwarf mass interval $0.5\text{--}0.7 M_{\odot}$, the shape of the WDLF is governed by cooling physics, while the SFR affects only the overall normalization. This result is in line with the analytical demonstration found in [80].

4 Impact of the axion emission in the WDLF

To assess the impact of axion emission on the shape of the WDLF, we computed theoretical WDLFs assuming different values of the axion–electron coupling constant g_{ae} . In line with the discussion in the previous sections, comparisons between the *Gaia* 100 pc WDLF and its theoretical counterparts are more robust when restricted to the region delimited by the 0.5 and $0.7 M_{\odot}$ cooling tracks and to magnitudes $M_G < 11.5$.

In this luminosity regime, the WDLF is expected to be largely insensitive to fluctuations in the local SFR on Gyr timescales, as suggested by different observational determinations of the Galactic disk SFR. We have empirically tested this expectation by considering a wide range of SFR models, from constant histories to bursty scenarios with different ages. We then evaluated how different stellar age bins populate the WDLF as a function of M_G (see Sec. 3.3). We found that the percentile relations between age bins remain nearly invariant up to $M_G \sim 11.5$, indicating that variations in the SFR have a negligible impact on the WDLF in this magnitude range.

Therefore, in what follows, we adopt WDLFs constructed under the assumption of a constant SFR, normalized to reproduce the theoretical WDLF in the range $9 < M_G < 11.5$.

The χ^2 -tests for every dataset analyzed in this section was computed via Python’s *scipy* library, which applies Pearson’s χ^2 -test as:

$$\chi^2 = \sum_{i=1}^N \frac{(O_i - E_i)^2}{E_i} ; \nu = N - 1, \quad (4.1)$$

where E_i are the expected counts, O_i the observed counts, N is the total number of bins, and $\nu = N - 1$ are the degrees of freedom, given that normalization is a fitted parameter. In order to properly estimate the theoretical expected values E_i , the theoretical realizations of the WDLF have been performed with a large sample of white dwarfs ($n \sim 10^5$). For each theoretical WDLF we have then computed the corresponding *p-value*, i.e. the right-tail probability of observing a χ^2 value greater than the one calculated under the null hypothesis,

$$p\text{-value} = P(\chi^2 \geq \chi_{\text{obs}}^2). \quad (4.2)$$

The theoretical WDLFs for different values of the axion-electron coupling constant g_{ae} in the $9 < M_G < 11.5$ range display very good agreement with the observations when considering $g_{ae} = 0$ —i.e. no axion emission—and for values of g_{ae} up to roughly $\sim 0.7 \times 10^{-13}$. Beyond this point, the fits deteriorate rather abruptly. A comparison of the WDLFs for these models is shown in Fig. 6 and the detailed statistical results are presented in Fig. 7. For the χ^2 -tests, several binning schemes were explored, all of them based on horizontal cuts in the magnitude axis, particularly binning schemes uniformly separated in M_G and schemes where the bins had equal number of stars. All possible results from this schemes are well constrained by the results shown in Fig. 7, regardless of the fact that the figure exhibits only

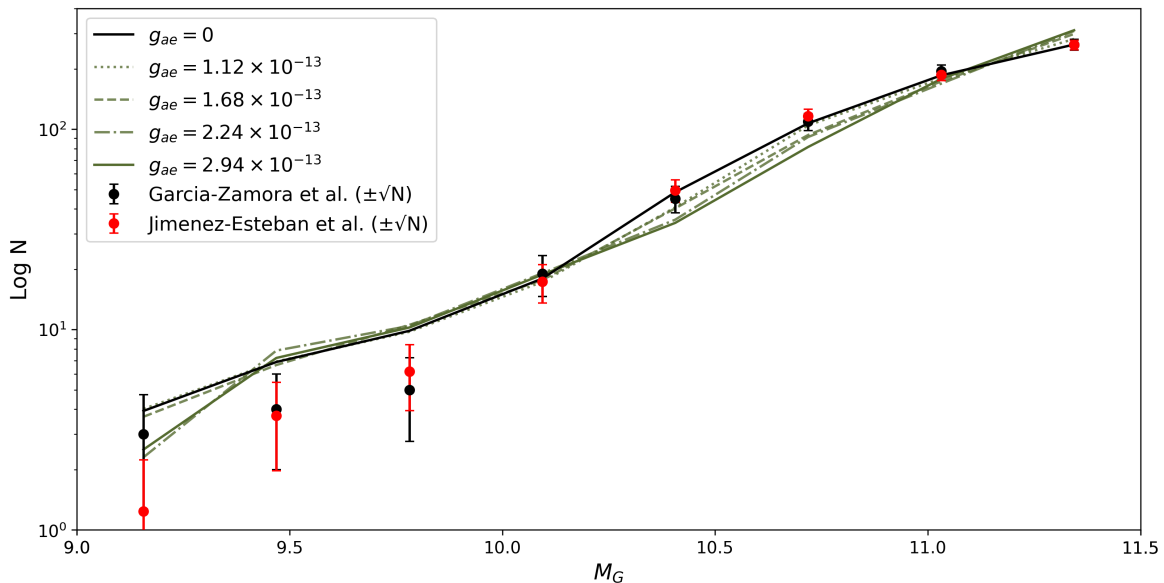


Figure 6. WDLFs in the $9 < M_G < 11.5$ range for different values of g_{ae} . In black and red dots the observed values, using Garcia-Zamora et al. DA sample [29] and —normalized to [29]— the Jimenez-Esteban et al. [28] DA sample, respectively.

schemes with roundly equal number of stars per bin. We conclude that values of g_{ae} greater than 1.68×10^{-13} can be discarded at 95% C.L. and values exceeding 2.52×10^{-13} at the 99.7% C.L.

5 Conclusions and future work

We have derived new constraints for the DFSZ-axion using *Gaia* DR3 and white dwarf luminosity functions constructed with synthetic white dwarf populations through a Monte Carlo code. We integrated into the code 360 state-of-the-art white dwarf cooling sequences, where the axion emission was computed self-consistently with the thermal structure of the stars. We improve upon previous constraints on the axion–electron coupling constant derived from the WDLF in two main ways:

1. By constructing a theoretical WDLF with a Monte Carlo code (see Sec. 3.1), rather than relying on a semi-analytical approach, as seen in [15, 16]. This methodology allows us to account for *Gaia* observational biases and selection criteria more effectively.

2. By exploiting the reliability of the *Gaia* DR3 100 pc volume-limited sample. In contrast, [15, 16] employed catalogs such as [81, 82], which were constructed via proper motion methods and through magnitude-limited samples, therefore inheriting the uncertainties associated with these approaches in the determination of the WDLF.

Together, these improvements in both the theoretical modeling and the observational data set allow us to derive significantly more robust constraints than those obtained in earlier works.

Let us summarize our findings:

1. The obtained g_{ae} constraints were $g_{ae} < 1.12 \times 10^{-13}$ at 68% C.L.; $g_{ae} < 1.68 \times 10^{-13}$ at 95% C.L.; and $g_{ae} < 2.52 \times 10^{-13}$ at 99.7% C.L. (see Fig. 7). That translates, in terms of

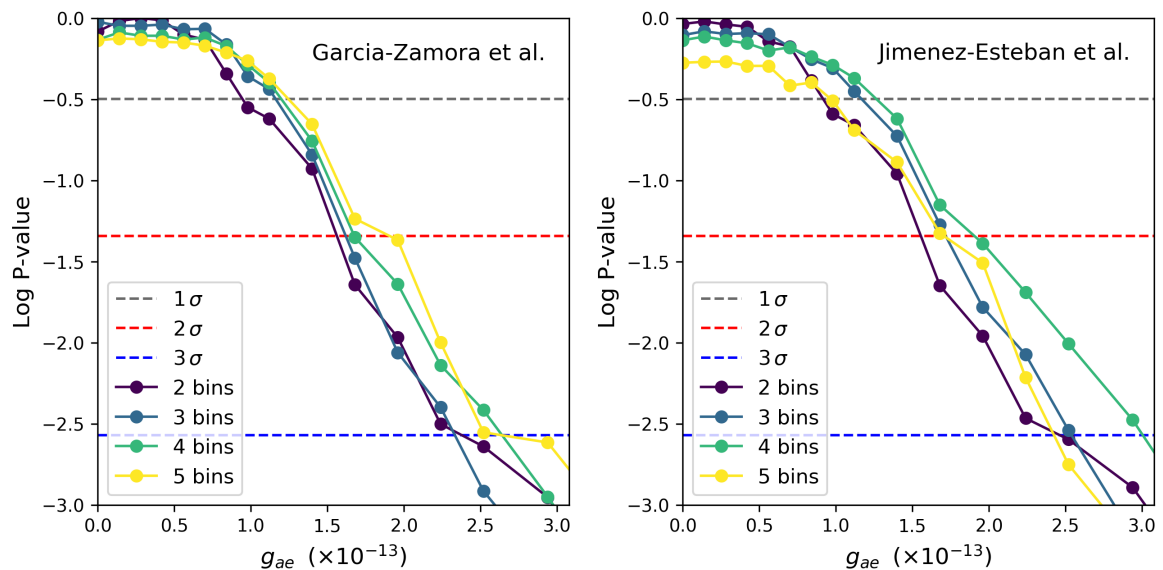


Figure 7. p -value as a function of g_{ae} for the brightest white dwarfs ($9 < M_G < 11.5$), using the samples of [28] (left panel) and [29] (right panel), and assuming a constant SFR. Different binning schemes are shown (2, 3, 4, and 5 bins), each constructed to contain roughly the same number of stars. The red and blue lines indicate the 2σ and 3σ confidence thresholds, respectively.

$m_a \cos^2 \beta$ through Eq. 1.1, to 4, 6, and 9 meV, respectively. These constraints were obtained under a conservative but robust approach, restricting the analysis to the brighter portion of the sample, where the effects of the uncertainties in the SFR are almost negligible.

2. Different binning schemes were explored, and in all the considered cases, the likeliness of the fits decreases relatively rapid as g_{ae} becomes greater than $\sim 0.7 \times 10^{-13}$.

3. In order to have a better statistical test coming from Galactic disk observations a good understanding of the SFR is needed (see Appendix A). A possible solution is to look for simpler populations. Recently, [83] have presented a study of the white dwarf cooling sequence of the globular cluster 47 Tuc using deep infrared observations with the JWST, and estimating the cluster age as 11.8 ± 0.5 Gyr.

In fact, our results are nearly a factor of two less constraining than the recent determination of [84], who analyzed white-dwarf cooling in the globular cluster 47 Tuc. This difference is consistent with our expectations: the dominant uncertainty in the Galactic-disk WDLF arises from the star-formation history, it seems natural that a stellar population with well-constrained distance, star-formation rate, and metallicity would yields stronger limits. Nevertheless, 47 Tuc represents a single cluster, and the resulting inference may be sensitive to cluster-specific systematics. In particular, the observed white-dwarf sequence is derived from specific regions of the outer field of 47 Tuc [85] and may be affected by position-dependent effects such as crowding and mass segregation. More generally, the unavoidable presence of unknown unknowns is a key consideration when assessing the robustness of astrophysical constraints on particle physics. These issues highlight the complementarity between field—and cluster—based approaches. Likewise, our bounds are comparable to, but complementary with, those derived from the TRGB [86, 87], which are subject to a very distinct set of systematic uncertainties. Besides the stellar formation rate, other limitations of this work include the neglect of mergers and binary evolution, and—on a more minor note—the

adopted Galactic scale height, and the omission of axion effects on stellar thermal structure from the main sequence onward. In this context, we note that [88] report that ALP couplings can affect the estimated ages of massive CO white dwarf progenitors and modify the IFMR, potentially influencing population synthesis studies. However, these effects are not relevant for our purposes, as the disk ages explored here are substantially larger than the variations introduced by these ALP-induced corrections.

As for future work, in [32] Bremsstrahlung emission formulas are provided, not only for axions, but also for baryophilic and leptophilic scalars, under the assumption of degenerate, semi-relativistic electrons and ion–ion correlations in the liquid phase. In the case of scalars, however, the WDLF should depart from the standard one at large M_G , rather than small ones. We plan to extend our analysis to these additional particles and incorporate them into future studies of the WDLF in stellar clusters such as 47 Tuc [83].

A Effects of stellar formation bursts on the WDLF

In Sec. 3.3, we discussed why the brightest portion of the WDLF, $M_G \lesssim 11.5$, is particularly well suited for robust statistical tests of additional cooling channels, such as axion emission via electron–ion bremsstrahlung. The same cannot be said when the analysis includes WDs dimmer than $M_G \sim 11.5$.

For instance, in Fig. 8 we show the WDLFs in the range $9 < M_G < 13$ for different values of g_{ae} , assuming a constant SFR, together with the corresponding p -values as a function of g_{ae} . Although the fits systematically worsen for larger values of the axion–electron coupling g_{ae} , none of the tests yields a good fit. Normalizing the counts over this magnitude range leads to an underestimation of the WDLF at $M_G \lesssim 11.5$, followed by an overestimation at the fainter end.

Reproducing such trends would require white dwarfs to cool more slowly in the bright part of the diagram, opposite to the effect expected from additional anomalous cooling due to axions. A more plausible explanation is that the shape of the observed WDLF can be reproduced by a localized enhancement of the SFR affecting the progenitors of WDs populating the brighter region of the color–magnitude diagram (see Fig. 5). As discussed in Sec. 3.3, sufficiently long-lived bursts do not affect the slope of the bright part of the WDLF ($M_G \lesssim 11.5$), but they increase the total number of WDs in that region and flatten the slope of the WDLF at fainter magnitudes ($M_G \sim 13$), thus improving the agreement with the data.

Indeed, we find that it is possible to reproduce the observed WDLF morphology by adopting a SFR with additional degrees of freedom. In particular, we obtain acceptable fits (p -value $\gtrsim 74$) for a model consisting of a constant SFR over 10.6 Gyr plus two Gaussian bursts (see Fig. 9). However, this model introduces several free parameters, including the mean age, width, and normalization of each burst, as well as the normalization of the constant component. This highlights a fundamental limitation of this approach: In order to use the WDLF to robustly constrain the axion–electron coupling, the SFR must be determined independently of the white dwarf sample; otherwise, the additional free parameters could be used to artificially improve or degrade the quality of the fits for different values of g_{ae} . Given the current uncertainties in the observational determination of the SFR in the solar neighborhood, this requirement appears difficult to satisfy.

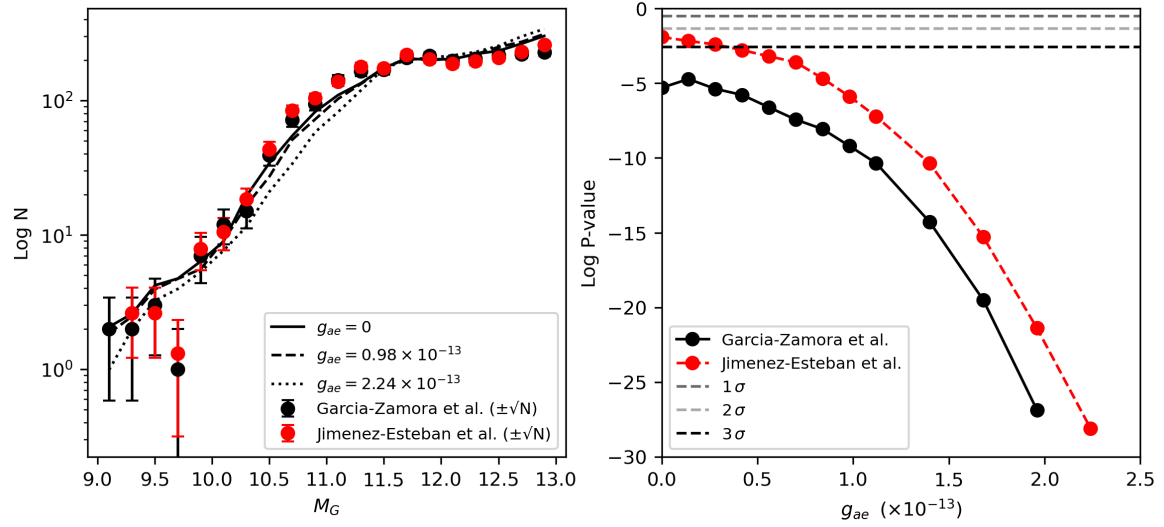


Figure 8. Left panel: with lines, the theoretical WDLFs on the range $9 < M_G < 13$, for different values of g_{ae} , using a constant SFR. Right panel: the p -values in function of the coupling constant g_{ae} .

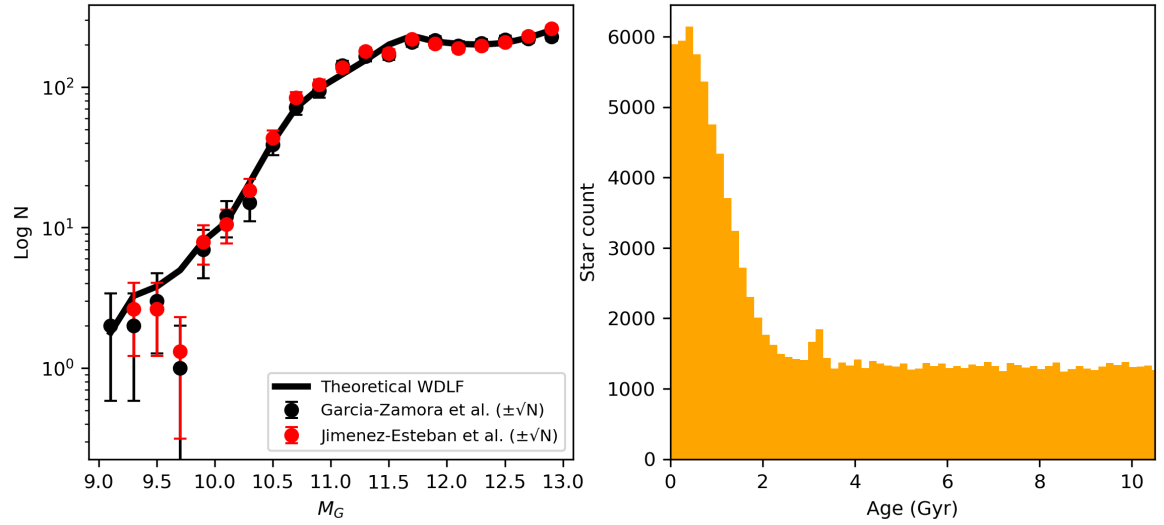


Figure 9. Left panel: WDLF adjustment using three constant SFR components. A main component of 10.6 Gyr and two bell-shaped bursts, resulting in a p -value $\gtrsim 74\%$. Right panel: the adjusted SFR.

Acknowledgments

MLA and MMB were supported by CONICET and Agencia I+D+i through grants PIP-2971 and PICT 2020-03316. MEC acknowledges grant RYC2021-032721-I, funded by MCIN/AEI/10.13039

/501100011033. MEC and ST were supported by the European Union Next Generation EU/PRTR, the AGAUR/Generalitat de Catalunya grant SGR-386/2021, and by the Spanish MINECO grant PID2023-148661NB-I00. AC is supported by an ERC STG grant (“Astro-

DarkLS”, grant No. 101117510). AC acknowledges the Weizmann Institute of Science for hospitality at different stages of this project and the support from the Benozziyo Endowment Fund for the Advancement of Science. MEC and ST acknowledge Jordi Isern for fruitful discussions.

References

- [1] R.D. Peccei and H.R. Quinn, *CP conservation in the presence of pseudoparticles*, *Phys. Rev. Lett.* **38** (1977) 1440.
- [2] S. Weinberg, *A new light boson?*, *Phys. Rev. Lett.* **40** (1978) 223.
- [3] F. Wilczek, *Problem of strong P and T invariance in the presence of instantons*, *Phys. Rev. Lett.* **40** (1978) 279.
- [4] P. Svrcek and E. Witten, *Axions In String Theory*, *JHEP* **06** (2006) 051 [[hep-th/0605206](#)].
- [5] A. Arvanitaki, S. Dimopoulos, S. Dubovsky, N. Kaloper and J. March-Russell, *String Axiverse*, *Phys. Rev. D* **81** (2010) 123530 [[0905.4720](#)].
- [6] I.G. Irastorza and J. Redondo, *New experimental approaches in the search for axion-like particles*, *Prog. Part. Nucl. Phys.* **102** (2018) 89 [[1801.08127](#)].
- [7] L. Di Luzio, M. Giannotti, E. Nardi and L. Visinelli, *The landscape of QCD axion models*, *Phys. Rept.* **870** (2020) 1 [[2003.01100](#)].
- [8] F. Chadha-Day, J. Ellis and D.J.E. Marsh, *Axion dark matter: What is it and why now?*, *Science Advances* **8** (2022) eabj3618 [[2105.01406](#)].
- [9] Y.K. Semertzidis and S. Youn, *Axion dark matter: How to see it?*, *Science Advances* **8** (2022) eabm9928 [[2104.14831](#)].
- [10] C.A.J. O’Hare, *Cosmology of axion dark matter*, *PoS COSMICWISPers* (2024) 040 [[2403.17697](#)].
- [11] A. Caputo and G. Raffelt, *Astrophysical Axion Bounds: The 2024 Edition*, *arXiv e-prints* (2024) [arXiv:2401.13728](#) [[2401.13728](#)].
- [12] P. Carena, M. Giannotti, J. Isern, A. Mirizzi and O. Straniero, *Axion astrophysics*, *Physical Research* **1117** (2025) 1 [[2411.02492](#)].
- [13] G.G. Raffelt, *Stars as laboratories for fundamental physics : the astrophysics of neutrinos, axions, and other weakly interacting particles*, University of Chicago Press (1996).
- [14] J. Isern, E. García-Berro, S. Torres and S. Catalán, *Axions and the Cooling of White Dwarf Stars*, *ApJ* **682** (2008) L109 [[0806.2807](#)].
- [15] M.M. Miller Bertolami, B.E. Melendez, L.G. Althaus and J. Isern, *Revisiting the axion bounds from the Galactic white dwarf luminosity function*, *J. Cosmology Astropart. Phys.* **2014** (2014) 069 [[1406.7712](#)].
- [16] J. Isern, E. García-Berro, S. Torres, R. Cojocaru and S. Catalán, *Axions and the luminosity function of white dwarfs: the thin and thick discs, and the halo*, *MNRAS* **478** (2018) 2569 [[1805.00135](#)].
- [17] A.H. Córscico, L.G. Althaus, M.M. Miller Bertolami, A.D. Romero, E. García-Berro, J. Isern et al., *The rate of cooling of the pulsating white dwarf star G117-B15A: a new asteroseismological inference of the axion mass*, *MNRAS* **424** (2012) 2792 [[1205.6180](#)].
- [18] A.H. Córscico, L.G. Althaus, A.D. Romero, A.S. Mukadam, E. García-Berro, J. Isern et al., *An independent limit on the axion mass from the variable white dwarf star R548*, *J. Cosmology Astropart. Phys.* **2012** (2012) 010 [[1211.3389](#)].

- [19] A.H. Córscico, A.D. Romero, L.G. Althaus, E. García-Berro, J. Isern, S.O. Kepler et al., *An asteroseismic constraint on the mass of the axion from the period drift of the pulsating DA white dwarf star L19-2*, *J. Cosmology Astropart. Phys.* **2016** (2016) 036 [[1605.06458](#)].
- [20] T. Battich, A.H. Córscico, L.G. Althaus and M.M. Miller Bertolami, *First axion bounds from a pulsating helium-rich white dwarf star*, *J. Cosmology Astropart. Phys.* **2016** (2016) 062 [[1605.07668](#)].
- [21] A.R. Zhitnitsky, *On Possible Suppression of the Axion Hadron Interactions. (In Russian)*, *Sov. J. Nucl. Phys.* **31** (1980) 260.
- [22] M. Dine, W. Fischler and M. Srednicki, *A Simple Solution to the Strong CP Problem with a Harmless Axion*, *Phys. Lett. B* **104** (1981) 199.
- [23] M. Schmidt, *Space Distribution and Luminosity Functions of Quasi-Stellar Radio Sources*, *ApJ* **151** (1968) 393.
- [24] H.C. Harris, J.A. Munn, M. Kilic, J. Liebert, K.A. Williams, T. von Hippel et al., *The White Dwarf Luminosity Function from Sloan Digital Sky Survey Imaging Data*, *AJ* **131** (2006) 571 [[astro-ph/0510820](#)].
- [25] S. De Gennaro, T. von Hippel, D.E. Winget, S.O. Kepler, A. Nitta, D. Koester et al., *White Dwarf Luminosity and Mass Functions from Sloan Digital Sky Survey Spectra*, *AJ* **135** (2008) 1 [[0709.2190](#)].
- [26] F.M. Jiménez-Esteban, S. Torres, A. Rebassa-Mansergas, G. Skorobogatov, E. Solano, C. Cantero et al., *A white dwarf catalogue from Gaia-DR2 and the Virtual Observatory*, *MNRAS* **480** (2018) 4505 [[1807.02559](#)].
- [27] S. Torres, C. Cantero, A. Rebassa-Mansergas, G. Skorobogatov, F.M. Jiménez-Esteban and E. Solano, *Random Forest identification of the thin disc, thick disc, and halo Gaia-DR2 white dwarf population*, *MNRAS* **485** (2019) 5573 [[1903.07362](#)].
- [28] F.M. Jiménez-Esteban, S. Torres, A. Rebassa-Mansergas, P. Cruz, R. Murillo-Ojeda, E. Solano et al., *Spectral classification of the 100 pc white dwarf population from Gaia-DR3 and the virtual observatory*, *MNRAS* **518** (2023) 5106 [[2211.08852](#)].
- [29] E.M. García-Zamora, S. Torres and A. Rebassa-Mansergas, *White dwarf Random Forest classification through Gaia spectral coefficients*, *A&A* **679** (2023) A127 [[2308.07090](#)].
- [30] O. Vincent, M.A. Barstow, S. Jordan, C. Mander, P. Bergeron and P. Dufour, *Classification and parameterization of a large Gaia sample of white dwarfs using XP spectra*, *A&A* **682** (2024) A5 [[2308.05572](#)].
- [31] P.-E. Tremblay, A. Bédard, M.W. O’Brien, J. Munday, A.K. Elms, N.P. Gentillo Fusillo et al., *The Gaia white dwarf revolution*, *New A Rev.* **99** (2024) 101705 [[2402.14960](#)].
- [32] S. Bottaro, A. Caputo, G. Raffelt and E. Vitagliano, *Stellar limits on scalars from electron-nucleus bremsstrahlung*, *J. Cosmology Astropart. Phys.* **2023** (2023) 071 [[2303.00778](#)].
- [33] M. Nakagawa, Y. Kohyama and N. Itoh, *Axion Bremsstrahlung in Dense Stars*, *ApJ* **322** (1987) 291.
- [34] M. Nakagawa, T. Adachi, Y. Kohyama and N. Itoh, *Axion Bremsstrahlung in Dense Stars. II. Phonon Contributions*, *ApJ* **326** (1988) 241.
- [35] L.G. Althaus, A.M. Serenelli, J.A. Panei, A.H. Córscico, E. García-Berro and C.G. Scóccola, *The formation and evolution of hydrogen-deficient post-AGB white dwarfs: The emerging chemical profile and the expectations for the PG 1159-DB-DQ evolutionary connection*, *A&A* **435** (2005) 631 [[astro-ph/0502005](#)].
- [36] I. Renedo, L.G. Althaus, M.M. Miller Bertolami, A.D. Romero, A.H. Córscico, R.D. Rohrmann et al., *New Cooling Sequences for Old White Dwarfs*, *ApJ* **717** (2010) 183 [[1005.2170](#)].

- [37] M.M. Miller Bertolami, L.G. Althaus and E. García-Berro, *Quiescent Nuclear Burning in Low-metallicity White Dwarfs*, *ApJ* **775** (2013) L22 [[1308.2062](#)].
- [38] L. Segretain, G. Chabrier, M. Hernanz, E. Garcia-Berro, J. Isern and R. Mochkovitch, *Cooling Theory of Crystallized White Dwarfs*, *ApJ* **434** (1994) 641.
- [39] G. Magni and I. Mazzitelli, *Thermodynamic properties and equations of state for hydrogen and helium in stellar conditions.*, *A&A* **72** (1979) 134.
- [40] S. Cassisi, A.Y. Potekhin, A. Pietrinferni, M. Catelan and M. Salaris, *Updated Electron-Conduction Opacities: The Impact on Low-Mass Stellar Models*, *ApJ* **661** (2007) 1094 [[astro-ph/0703011](#)].
- [41] C.A. Iglesias and F.J. Rogers, *Updated Opal Opacities*, *ApJ* **464** (1996) 943.
- [42] J.W. Ferguson, D.R. Alexander, F. Allard, T. Barman, J.G. Bodnarik, P.H. Hauschildt et al., *Low-Temperature Opacities*, *ApJ* **623** (2005) 585 [[astro-ph/0502045](#)].
- [43] R.D. Rohrmann, L.G. Althaus, E. García-Berro, A.H. Córscico and M.M. Miller Bertolami, *Outer boundary conditions for evolving cool white dwarfs*, *A&A* **546** (2012) A119 [[1209.2452](#)].
- [44] N. Itoh, H. Hayashi, A. Nishikawa and Y. Kohyama, *Neutrino Energy Loss in Stellar Interiors. VII. Pair, Photo-, Plasma, Bremsstrahlung, and Recombination Neutrino Processes*, *ApJS* **102** (1996) 411.
- [45] M. Haft, G. Raffelt and A. Weiss, *Standard and Nonstandard Plasma Neutrino Emission Revisited*, *ApJ* **425** (1994) 222 [[astro-ph/9309014](#)].
- [46] J.M. Burgers, *Flow Equations for Composite Gases*, New York: Academic Press (1969).
- [47] L.G. Althaus, A.H. Córscico, M. Uzundag, M. Vučković, A.S. Baran, K.J. Bell et al., *About the existence of warm H-rich pulsating white dwarfs*, *A&A* **633** (2020) A20 [[1911.02442](#)].
- [48] L.G. Althaus, A.H. Córscico and F. De Gerónimo, *Effect of Coulomb diffusion of ions on the pulsational properties of DA white dwarfs*, *A&A* **644** (2020) A55 [[2010.11131](#)].
- [49] G.G. Raffelt, *Axion constraints from white dwarf cooling times*, *Physics Letters B* **166** (1986) 402.
- [50] L.M. Krauss, J.E. Moody and F. Wilczek, *A STELLAR ENERGY LOSS MECHANISM INVOLVING AXIONS*, *Phys. Lett. B* **144** (1984) 391.
- [51] G.G. Raffelt, *ASTROPHYSICAL AXION BOUNDS DIMINISHED BY SCREENING EFFECTS*, *Phys. Rev. D* **33** (1986) 897.
- [52] G. Raffelt and A. Weiss, *Red giant bound on the axion-electron coupling reexamined*, *Phys. Rev. D* **51** (1995) 1495 [[hep-ph/9410205](#)].
- [53] P. Carena and G. Lucente, *Revisiting axion-electron bremsstrahlung emission rates in astrophysical environments*, *Phys. Rev. D* **103** (2021) 123024 [[2104.09524](#)].
- [54] M.M. Miller Bertolami, *New models for the evolution of post-asymptotic giant branch stars and central stars of planetary nebulae*, *A&A* **588** (2016) A25 [[1410.1679](#)].
- [55] L. Casagrande, R. Schönrich, M. Asplund, S. Cassisi, I. Ramírez, J. Meléndez et al., *New constraints on the chemical evolution of the solar neighbourhood and Galactic disc(s). Improved astrophysical parameters for the Geneva-Copenhagen Survey*, *A&A* **530** (2011) A138 [[1103.4651](#)].
- [56] M. Bergemann, K. Lodders and H. Palme, *The Chemical Composition of the Sun*, *arXiv e-prints* (2025) [arXiv:2503.05402](#) [[2503.05402](#)].
- [57] E. García-Berro, S. Torres, J. Isern and A. Burkert, *Monte Carlo simulations of the disc white dwarf population*, *MNRAS* **302** (1999) 173.

- [58] S. Torres, E. García-Berro, J. Isern and F. Figueras, *Simulating Gaia performances on white dwarfs*, *MNRAS* **360** (2005) 1381 [[astro-ph/0504409](#)].
- [59] S. Torres and E. García-Berro, *The white dwarf population within 40 pc of the Sun*, *A&A* **588** (2016) A35 [[1602.02533](#)].
- [60] S. Torres, A. Rebassa-Mansergas, M.E. Camisassa and R. Raddi, *The Gaia DR2 halo white dwarf population: the luminosity function, mass distribution, and its star formation history*, *MNRAS* **502** (2021) 1753 [[2101.03341](#)].
- [61] J. Camacho, S. Torres, E. García-Berro, M. Zorotovic, M.R. Schreiber, A. Rebassa-Mansergas et al., *Monte Carlo simulations of post-common-envelope white dwarf + main sequence binaries: comparison with the SDSS DR7 observed sample*, *A&A* **566** (2014) A86 [[1404.5464](#)].
- [62] R. Cojocaru, A. Rebassa-Mansergas, S. Torres and E. García-Berro, *The population of white dwarf-main sequence binaries in the SDSS DR 12*, *MNRAS* **470** (2017) 1442 [[1705.05888](#)].
- [63] P. Canals, S. Torres and N. Soker, *Oxygen-neon-rich merger during common envelope evolution*, *MNRAS* **480** (2018) 4519 [[1806.06730](#)].
- [64] S. Torres, P. Canals, F.M. Jiménez-Esteban, A. Rebassa-Mansergas and E. Solano, *A population synthesis fitting of the Gaia resolved white dwarf binary population within 100 pc*, *MNRAS* **511** (2022) 5462 [[2202.04199](#)].
- [65] E. García-Berro, S. Torres, L.G. Althaus, I. Renedo, P. Lorén-Aguilar, A.H. Córscico et al., *A white dwarf cooling age of 8Gyr for NGC 6791 from physical separation processes*, *Nature* **465** (2010) 194 [[1005.2272](#)].
- [66] S. Torres, E. García-Berro, L.G. Althaus and M.E. Camisassa, *The white dwarf population of NGC 6397*, *A&A* **581** (2015) A90 [[1507.08806](#)].
- [67] S. Torres, E. García-Berro, R. Cojocaru and A. Calamida, *The population of single and binary white dwarfs of the Galactic bulge*, *MNRAS* **476** (2018) 1654 [[1802.00229](#)].
- [68] E.E. Salpeter, *The Luminosity Function and Stellar Evolution.*, *ApJ* **121** (1955) 161.
- [69] A. Pietrinferni, S. Cassisi, M. Salaris and F. Castelli, *A Large Stellar Evolution Database for Population Synthesis Studies. I. Scaled Solar Models and Isochrones*, *ApJ* **612** (2004) 168 [[astro-ph/0405193](#)].
- [70] J.D. Cummings, J.S. Kalirai, P.-E. Tremblay, E. Ramirez-Ruiz and J. Choi, *The White Dwarf Initial-Final Mass Relation for Progenitor Stars from 0.85 to 7.5 M_{\odot}* , *ApJ* **866** (2018) 21 [[1809.01673](#)].
- [71] A. Rebassa-Mansergas, J. Maldonado, R. Raddi, A.T. Knowles, S. Torres, M. Hoskin et al., *Constraining the solar neighbourhood age-metallicity relation from white dwarf-main sequence binaries*, *MNRAS* **505** (2021) 3165 [[2105.13379](#)].
- [72] D. Koester, *White dwarf spectra and atmosphere models*, *Mem. Soc. Astron. Italiana* **81** (2010) 921.
- [73] M. del Alcázar-Julìà, F. Figueras, A.C. Robin, O. Bienaymé and F. Anders, *Joint inference of the Milky Way's star formation history and initial mass function from Gaia all-sky $G \pm 13$ data*, *A&A* **697** (2025) A128 [[2501.17236](#)].
- [74] A. Zubiaur, R. Raddi and S. Torres, *Kinematic origin of white dwarfs in the solar neighborhood*, *A&A* **687** (2024) A286 [[2405.10380](#)].
- [75] R. Mor, A.C. Robin, F. Figueras, S. Roca-Fàbrega and X. Luri, *Gaia DR2 reveals a star formation burst in the disc 2-3 Gyr ago*, *A&A* **624** (2019) L1 [[1901.07564](#)].
- [76] J. Isern, *The Star Formation History in the Solar Neighborhood as Told by Massive White Dwarfs*, *ApJ* **878** (2019) L11 [[1905.10779](#)].

- [77] E. Cukanovaite, P.-E. Tremblay, S. Toonen, K.D. Temmink, C.J. Manser, M.W. O'Brien et al., *Local stellar formation history from the 40 pc white dwarf sample*, *MNRAS* **522** (2023) 1643 [2209.13919].
- [78] H.-R. Noh and J. Scalo, *History of the Milky Way Star Formation Rate from the White Dwarf Luminosity Function*, *ApJ* **352** (1990) 605.
- [79] J. Isern, E. García-Berro, S. Torres and S. Catalán, *Axions and the Cooling of White Dwarf Stars*, *ApJ* **682** (2008) L109 [0806.2807].
- [80] J. Isern, S. Catalán, E. García-Berro and S. Torres, *Axions and the white dwarf luminosity function*, in *Journal of Physics Conference Series*, vol. 172 of *Journal of Physics Conference Series*, p. 012005, IOP, June, 2009, DOI [0812.3043].
- [81] N. Rowell and N.C. Hambly, *White dwarfs in the SuperCOSMOS Sky Survey: the thin disc, thick disc and spheroidal luminosity functions*, *MNRAS* **417** (2011) 93.
- [82] H.C. Harris, J.A. Munn, M. Kilic, J. Liebert, K.A. Williams, T. von Hippel et al., *The White Dwarf Luminosity Function from Sloan Digital Sky Survey Imaging Data*, *AJ* **131** (2006) 571 [astro-ph/0510820].
- [83] M. Salaris, M. Scalco, L. Bedin and S. Cassisi, *James Webb Space Telescope observations of the white dwarf cooling sequence of 47 Tucanae*, *MNRAS* **541** (2025) 1390 [2506.20732].
- [84] L. Fleury, A. Obertas, H. Richer and J. Heyl, *Axion Constraints from White Dwarf Cooling in 47 Tucanae*, 2511.21676.
- [85] J.S. Kalirai, H.B. Richer, J. Anderson, A. Dotter, G.G. Fahlman, B.M.S. Hansen et al., *A Deep, Wide-field, and Panchromatic View of 47 Tuc and the SMC with HST: Observations and Data Analysis Methods*, *AJ* **143** (2012) 11 [1112.1426].
- [86] N. Viaux, M. Catelan, P.B. Stetson, G.G. Raffelt, J. Redondo, A.A.R. Valcarce et al., *Neutrino and Axion Bounds from the Globular Cluster M5 (NGC 5904)*, *Phys. Rev. Lett.* **111** (2013) 231301 [1311.1669].
- [87] F. Capozzi and G. Raffelt, *Axion and neutrino bounds improved with new calibrations of the tip of the red-giant branch using geometric distance determinations*, *Phys. Rev. D* **102** (2020) 083007 [2007.03694].
- [88] I. Domínguez, O. Straniero, L. Piersanti, M. Giannotti and A. Mirizzi, *The impact of axion-like particles on late stellar evolution: From intermediate-mass stars to core-collapse supernova progenitors*, *A&A* **702** (2025) A240 [2508.17779].